IET Smart Grid

Special Issue: Definition, Quantification, Analysis and Enhancement of Grid Resilience

IET Journals
The Institution of Engineering and Technology

Quantification and visualisation of extreme wind effects on transmission network outage probability and wind generation output

eISSN 2515-2947
Received on 5th June 2019
Revised 29th August 2019
Accepted on 26th September 2019
E-First on 2nd April 2020
doi: 10.1049/iet-stg.2019.0145
www.ietdl.org

Magnus R. Jamieson[1] ✉, Goran Strbac[1], Keith R.W. Bell[2]

[1]*Control and Power Group, Imperial College London, South Kensington, London, UK*
[2]*Department of Electrical Engineering, University of Strathclyde, Glasgow, UK*
✉ *E-mail: m.jamieson16@imperial.ac.uk*

Abstract: An approach is demonstrated to visualise overhead line failure rates and estimated wind power output during extreme wind events on transmission networks. Reanalysis data is combined with network data and line failure models to illustrate spatially resolved line failure probability with data corrected for asset altitude and exposure. Wind output is estimated using a corrected power curve to account for high speed shutdown with wind speed corrected for altitude. Case studies demonstrate these methods' application on representations of real networks of different scales. The proposed methods allow users to determine at-risk regions of overhead line networks and to estimate the impact on wind power output. Such techniques could equally be applied to forecasted weather conditions to aid in resilience planning. The methods are shown to be particularly sensitive to the weather data used, especially when modelling risk on overhead lines, but are still shown to be useful as an indicative representation of system risk. The techniques also provide a more robust method of representing weather-related failure rates on lines considerate of the altitude, voltage level, and their varying exposure to weather conditions than current techniques typically provide, which can be used to usefully represent failure probability of lines during storms.

1 Introduction

Extreme weather and climate change manifest as risks for the power system in multiple ways which are difficult to quantify, and challenging to productively address. Climate change itself will manifest as changing both the frequency and intensity of extreme weather events such as storms, droughts, hurricanes, and heatwaves [1].

In power systems, this means changing probabilities of weather-related outages on networks as well as changes to the availability and resilience of energy resources on which renewable energy vectors are reliant [2]. Further, climatological phenomena which drive wind may change, affecting wind resources in countries such as the UK [3].

The above factors mean tools are needed to be able to quantify the effects of these phenomena on the power system in an understandable and productive way for system operators and planners – but these approaches also need to be robust and data-driven to reduce the risk of stranded assets and waste. Given the wide variety of natural hazards which can affect power systems, from floods to wildfires, such methodologies should also be portable to other sets of weather phenomena. This paper is primarily concerned with the impact that extreme winds have on the operation of a power system.

Wind can cause mechanical failure of conductors and connectors, or debris from vegetation can cause common-mode faults disconnecting wide sections of the system for extended periods of time [4] – but this risk will vary not just across systems but between individual lines, particularly if they traverse mountainous or coastal regions. For example, in the UK, the tree-line varies from 530 to over 600 m [5], subject to land use and local conditions. Therefore, if a network branch traverses regions above this elevation, it will not be so vulnerable to faults associated with collapsing vegetation – but that elevation could mean they are more exposed to hazardous weather conditions associated with e.g. lightning, which requires different forms of analysis [6]. Current methodologies cannot typically capture this variation. Conversely, low-lying regions in the UK are susceptible to flooding, with large-scale outages associated with inundations of distribution equipment [7]. Southerly regions also tend to be less windy, due to complementary climatological patterns [8].

Understanding comprehensively risk associated with extreme weather is important because it affects the ability of companies and individuals to plan for resilience. An analysis of resilience and its definitions is carried out in [9], the general themes of which relate to the ability of a system to prevent, contain and recover from adverse impacts arising from unplanned or extreme events. Resilience analysis has to consider both the impact and probability of an event.

Resilience impacts associated with extreme wind have been investigated in work such as [10], but the representations of risk on lines used have not been truly representative of localised wind impacts, but rather utilise homogenous representations of network branches. These are generally considerate only of wind speeds experienced at nodes rather than localised weather conditions, which can vary significantly across network branches. Wind power output, too, can also be significantly affected by extreme wind as storms pass across wind farms and regions [11]. Therefore, wind-related risk on overhead lines (OHLs) and wind power output are intrinsically linked concepts but in order to fully understand the interaction between these elements there needs to be an appropriately disaggregated spatiotemporal analysis.

This paper concentrates on how to represent and model wind-related failure rates on OHL networks and the potential links between system risk and wind power availability during storm events. These methods also begin to take consideration of the impact of the different geographic conditions a network branch may cover and the diversity of weather it may be subjected to in a way comparable studies have not. The proposed methodology, therefore, demonstrates an approach for quantifying the threats associated with adverse weather conditions which can be adapted for different natural hazards to understand how threats to OHL may vary regionally. Disaggregating such representations of network branches could allow operators and planners to determine not just which network branches are particularly at risk, but where on the network they are most likely to fault, allowing for more optimised placement of repair assets and teams.

Different approaches for modelling OHL faults on systems are described in Section 2. Section 3 describes the methodology used

to link wind speed to the failure rates on OHL; Section 4 concerns how to correct that wind data based on the given altitude of an asset with Section 5 relating this corrected wind speed to a projection of wind power output. The method is demonstrated on different representations of the GB network (that is, the mainland UK interconnected transmission system) in storm conditions to demonstrate the principles in Section 6 and Section 7 discusses the potential significance of network elevation to system security. This shows a clear advancement in the representation of line faults in security assessments, while also demonstrating the varied strength of different levels of network and the need to distinguish between such networks in analysis.

2 Approaches to representing failures on overhead lines

Modelling of line related failures due to weather events may typically fall into one of two different approaches. Historically and conventionally this has involved the use of different failure rates based on predefined 'regimes' such as 'normal', 'adverse/stormy', or 'extreme' failure rates representative of different weather states (such as in [12, 13]), or the use of 'fragility curves' which represent some link between a given weather parameter – in this case wind – and failure probability. The former approach has been used for some time, is relatively straightforward, and is codified in IEEE standards [14] – but has various flaws. These relate to how one actually defines when exactly a weather event goes from being 'normal' to 'adverse' or 'extreme', and how robust these distinctions are, particularly in the context of discussing extreme weather events and high impact low probability events. Furthermore, they also cannot capture regional variations across the system as in typical applications of this approach the same weather state is assumed to apply across the whole system. Although the use of such failure rates may be a simple approximation that is useful for reliability studies, in the context of resilience, more robust modelling of these kinds of risks is needed than is offered by such methods.

Fragility curves are a more data-driven approach which rely on, for instance, the use of Bayesian methods to calculate the probability of a fault on a given system asset experiencing a given condition, but in this case, the focus is particularly related to wind-related faults. This has been explored in some depth already in papers such as [15–17] with some investigation of, for instance, remediation strategies based on extensive Monte-Carlo simulation. An examination of different kinds of fragility curves and their derivations is also discussed in [18]. The curves used herein would fall under the category of being considered empirical fragility curves, according to the definitions offered therein. That is, based on real data. An example of the formulation of such a fragility curve is demonstrated in [19] based on an investigation of fault data pertaining to Northern Scotland. This shall be described further in Section 3.

The strength of fragility curves is that they are versatile and can be easily applied computationally in Monte-Carlo simulations, which are the prevalent form of reliability and resilience planning in more recent times. That is, the natural hazard being used to determine the failure probability of a given asset can simply be replaced to change the style of analysis; e.g. wind speed could be replaced with precipitation or some variable representative of lightning strike rates.

Fragility curves, however, bring with them separate challenges and problems compared to more general 'regimes' described before. The data required to derive them may be difficult to acquire or incomplete in nature. Further, at the long tail of the data, that is, at extreme values of e.g. wind speed, the data becomes incredibly sparse. This is a reason for the need for larger bins at extreme values of wind speed in [20] when classifying data at the long tail. They also assume a certain level of homogeneity of the assets being modelled and while, on average, the curve may be a reasonable approximation for the failure properties of a class of asset, the data can always be refined further. The data available for projections of future wind conditions may differ slightly from that used to derive them, requiring corrections to mitigate any systemic error introduced.

Factors such as the age of an asset may affect its resistance to wind-related failure, as will factors such as proximal vegetation, the elevation of such lines, and wind direction, which is ignored in the generation of these fragility curves. For example, lines in areas above the natural tree-line of a region may be more susceptible to landslips following heavy rain due to the lack of trees; but incorporating such factors in the analysis again faces data collection challenges as discriminating in such a manner further limits the scale of data available. For the purposes considered here, such curves can be considered useful for giving indicative representations of failure probabilities of lines, even if their precision may remain open to question in the manner such as they are being applied here. This highlights a major challenge with any kind of large-scale power system resilience analysis – the collection and application of appropriate weather data requires vigilance and a solid understanding of the relationships between the output models and the incident data to ensure appropriateness.

3 Modelling relationships between weather and line outages

The approach taken to modelling wind-related failure probability on lines in this paper uses fragility curves based on work from [19, 20]. In [19], a representative fragility curve was developed by analysing fault data in the Scottish Hydro Electric Transmission Ltd. (SHETL) region of the GB network, in the North of Scotland, and using it to develop a cumulative probability curve w.r.t wind speed. This is further developed in [20] to break the fragility curves down by voltage level. The value of the work performed in [20] is not only in the derivation of the curves themselves but in that they are broken down per 100 km, which allows failure rates to be determined when weighting according to exposure to different natural hazards.

The curves in this study are taken from the data tables in [20] pertaining to wind-related faults only, but considering '132 kV' lines and '275 and 400 kV' lines (the latter two of which are treated using the same fragility curve for the purposes of this study), based on the same bins as are used in the data tables. Given the sparsity of available data for faults on 275 and 400 kV lines, it is assumed the data for 275 kV lines are broadly applicable to 400 kV lines across GB. These fragility curves are shown in Fig. 1. The 'stepped' nature of the curves is due to the bins of data used in the source data.

3.1 Determining line exposure to weather conditions

In order to determine the risk across a line given a set of weather data, the actual level of exposure a certain line has to a given set of weather conditions has to be known. Previous work on this has assumed that the wind speed experienced by a given line can be assumed to be, for instance, the highest wind speed at either end of a given line. That is the wind speed measured at the buses on either side of a connection such as in [21]. Alternatively, each bus can be assigned to a weather 'region' and lines are assumed to experience the wind speeds of the highest value for the region in which they fall [10].

This is a reasonable first approximation, but for particularly long lines, which may traverse diverse geographical and meteorological conditions, this may not be an adequate approximation and may introduce significant error to failure rate calculations by either overestimating or underestimating the actual exposure of a line to a given weather condition. To address this, some link needs to be made between the weather data being used and the projection of lines through this weather data to determine what the actual nature of the exposure of a given line is to the observed weather conditions. In this context, 'exposure' refers to the length of OHL which is used as the value to correct the failure rate. The failure rate itself is taken from the fragility curve derived from the incident weather upon that line. For instance, an OHL going directly East for 100 km in a grid with 50 km × 50 km resolution from the far West of the first block could be understood

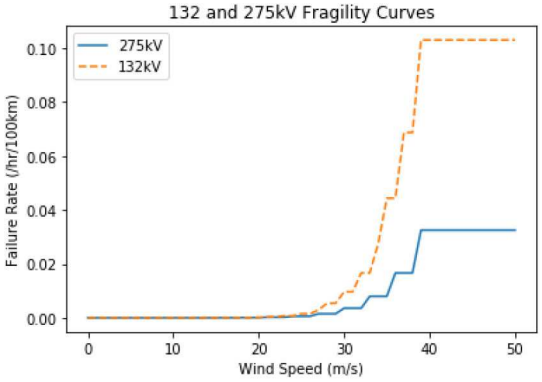

Fig. 1 *OHL fragility curves used in the proposed study*

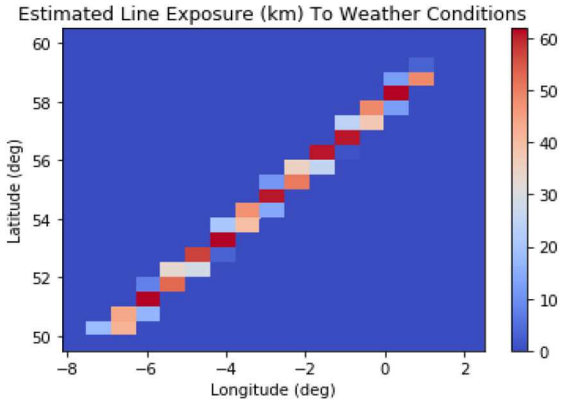

Fig. 2 *Example line exposure estimation for an OHL*

as constituting two blocks with 50 km in each. Each of these blocks would have a weather parameter associated with it and then an associated failure rate derived thereof. Correspondingly, an underground cable would have 0 exposure to the wind in all blocks. This will again be dependent on the weather parameter being analysed; if the study pertained to, for instance, temperature data this exposure characteristic would be computed and applied differently.

3.2 Converting co-ordinate set to two-dimensional (2D) data table

Determination of the exposure of each line in the system was achieved using a method created in *python*. Two, points at a given set of latitude and longitude are projected through 2D space and are given a consistent set of co-ordinates in the latitudinal and longitudinal directions. It can then be determined as to how much of a 'line' falls within the co-ordinate boundaries of a given set.

The co-ordinate data set used in this case is based on NASA MERRA-2 (Modern-Era Retrospective analysis for Research and Applications) [22] data, which resolves to 0.5° in latitude by 0.625° in longitude, or approximately 50 km × 50 km blocks. In order to determine how much 'line' was in each block of data, for two given nodes and a connected line, the script takes the two co-ordinates, treats this as a vector, and iterates through the vector in 1000 steps. The script then counts how many 'steps' are recorded in each block of weather-grid based data, and, using Pythagoras' theorem and the data resolution, converts this to a km length in each block – the 'exposure'. This effectively converts the co-ordinate set into a 2D representation in a *2D dataframe* [23] where each block for any given line represents the estimated amount of line in that area, information which can then be productively used.

A visual representation of an arbitrary OHL connecting two points is shown in Fig. 2. Each block represents how much of that 'line' is in that given block. Two different weather data sets will be used in this paper for comparison and will be described more fully in Section 6. Individual lines can be represented and analysed in this matter for power system simulations – that is, each block of a line can be sampled in turn to determine if a fault has occurred and where – or such representations can be aggregated across the system to perform more gross analyses.

3.3 Converting failure probability to failure rate to correct for length

The fragility curves in the source data stipulate failure probability in terms of every 100 km/h, agnostic of direction. In each 'block' of weather data a given line is treated as an aggregated, homogenous line exposed to the wind conditions, which have been assigned to that 'block' of data. This means the given failure probability determined by the source fragility curves had to be corrected to the actual exposure of the line in any given block to the weather. The primary difference between the application herein and that used to create the curves in [20] is that the weather data used to create the fragility curves was based on 3 hourly input resolution, on the assumption a fault would be caused by the maximum wind speed in that window. Conversely, as they were based on the wind speed at 10 m, this may also be a systemic underestimation of what the wind speed that caused the fault on the OHL actually was due to the fact that towers can be considerably taller than 10 m. The projection of failure rates herein uses hourly-resolved wind data at various different heights with different corrections. This made comparison across data sets important to determine potential sensitivity to changes in input data.

Similarly, using an average rather than a maximum value of wind may also constitute a systematic underestimation of incident wind speeds. Were features such as wind direction to be considered this could become even more problematic as the fragility curves as defined are agnostic of direction and thus to cross-utilise the curves may not be appropriate. While the implementation herein differs slightly from the derivation of the curves themselves, the data is deemed to be appropriate enough to provide an acceptable relative representation of system risk, as the models are applied consistently around the system.

To determine the actual failure probability of a given line in a given block of data, an exponential distribution of faults was assumed. The failure probability stipulated by the source fragility curve can then be converted to a failure rate in terms of every 100

km, then corrected for the actual length of line present in each block, then converted back into a failure probability – this is why Fig. 1 is shown w.r.t failure rate rather than probability, as fragility curves typically are.

It is assumed that the failure probability for a given line is represented by the standard equation for an exponential failure probability distribution as shown below

$$p(\text{fault}) = 1 - \mathrm{e}^{-\lambda \delta t} \tag{1}$$

Here, $p(fault)$ refers to the fault probability within a given time-step, λ is a failure rate, and δt is the given time step. δt is assumed to be 1 (i.e. 1 h) and the failure rate is given in per-hour terms. This can be rearranged to solve for λ for the given fragility curve to form an equivalent failure rate–wind speed conversion. This rate is then linearly scaled to correct for the actual exposure of a line in each block of data, and then can be converted back to failure probability.

The demonstrated combination of approaches can be used to create a representation of line risk across a network in given weather conditions both individually and, if representative data frames representing different lines are aggregated, at a system level. However, the robustness of the weather data on which our failure probabilities are based still needs to be considered. Two data sets will be used to demonstrate the sensitivity of models to incident wind data.

4 Correcting spatial wind speed data for various applications

MERRA-2 data take various different forms but in general, is reanalysis – or hindcasted – data which represents an estimation of the weather conditions at a point in space and time. MERRA-2 was chosen for its excellent balance between completeness, temporal and spatial resolution. Even then, selecting the specific subset of data to use introduces its own technical challenges.

Two different subsets are used, one which was based on u (East–West) and v (North–South) components of wind speed at 2, 10, and 50 m heights [24] (referred to herein as the 'three level' data), and the other which provides only a value for 'single level' maximum wind speed [25].

It is also useful to understand the geographic conditions which a line experiences as this will affect the ways in which a line may fail. For comparison, and to understand the geographic diversity of the test networks, the elevation of the test network is also investigated. As an example, this allows distinction between areas which may be at risk from large vegetation faults to be distinguished from more low-lying regions which may be more susceptible to flooding.

4.1 Determining elevation at given co-ordinate sets

MERRA-2 data assumes a 'smoothed' terrain with a given horizontal displacement. For wind speeds, particularly in geographically diverse regions like Highland Scotland, this may not be an appropriate approximation given the variable topological conditions and the corresponding impact on wind speeds and failure mechanics, particularly if one is only using homogenous representations of OHL. The mechanisms by which wind causes an OHL failure will be sensitive to the environment in which a line exists; above the tree line, for instance, the probability of a vegetation-related fault may differ significantly from an OHL which passes through an urban or forested region.

A method is therefore needed to quickly determine the elevation of a given point given a latitude–longitude co-ordinate pair. This was done using NASA Shuttle Radar Topographic Mission (SRTM) elevation data taken from [26]. This provided elevation data in the format of .tif images, which were then referenced using an API (application programming interface) provided by [27] which simply converted data from the associated .tif images to an elevation value for a given co-ordinate pair.

When creating the route data frames for the line projections, the elevation at every co-ordinate point can then be determined simply by calling the API at each point. This in itself introduces its own challenges – given a series of elevations within a block, an assumption still needs to be made to decide which values to use. As the context is one of resilience and reliability, it was deemed that it would be most appropriate to be conservative and treat each block as travelling through the highest observed elevation within that block.

4.2 Correcting wind speed for altitude of asset

The MERRA-2 data can then be corrected for the asset height of a given tower or turbine. For the case studies in question, wind turbine hub heights are assumed to be 100 m, with 132 kV OHL 30 m and 275 and 400 kV OHL approximated to 50 m, based on typical values of wind turbines and towers in the SHETL system – but in reality OHL heights and hub heights of turbine can vary significantly. This in itself carries various assumptions, given the diversity of wind turbine hub heights and OHL tower types, but was deemed an acceptable assumption for the purposes here.

An approach similar to that defined in [28] is used to correct wind speeds on various assets. That is, at each point, the $(2 + d)$m, $(10 + d)$m, and 50 m u and v components are found, and Pythagoras' theorem is used to resolve to resultant wind speed w, where d is the horizontal displacement of the MERRA-2 data in the given block. These values are then regressed against the log of their altitude. The wind speed at height h can then be estimated using

$$w(h) = A\log(h - d) - A\,\log(z) \tag{2}$$

In this equation, $w(h)$ is the wind speed w (ms^{-1}) at height h (m), or the asset anemometer height at which wind speed is measured A is determined by the slope of this regression, and z is calculated via

$$z = e^{-c/A} \tag{3}$$

In (3), c is the intercept of the given regression. Now the estimated wind speed experienced by an asset, and a relationship between this wind speed and the probability of failure of that asset, are known. The failure risk of a line can then be determined spatially or aggregated across a system. Such findings can then be compared between the single-level results and 3-level results corrected for height in this way.

4.3 Interpolation of weather data grid

To improve the granularity of the data an interpolation algorithm was used. This was taken from the python library *SciPy* [29], and is called *griddata*. This was used as it was accessible and usefully fast and efficient, adding little computational burden to the process. Where interpolation was used, the initial grid derived from the utilised weather data was linearly interpolated for five incremental blocks within each larger block. This differs from [28], where LOESS regression, specifically a 'non-parametric locally weighted scatterplot smoother', was used instead.

It was deemed in this work that only limited interpolation was needed to demonstrate what was happening, and so an algorithm which could be easily incorporated into the model was chosen, particularly given the more intense computational expense associated with increasing granularity. This interpolation does not fully account for topological variation, which in Scotland can be significant and is not captured by MERRA-2. This is effectively an extension of the Virtual Wind Farm model, described in [28], extended to apply to both wind farms and OHL.

5 Effects of wind speed on wind power output

High wind speed shutdown (HWSS) of wind farms can cause significant loss of infeed across geographic regions and has to be considered, and can be difficult to quantify given the diversity of conditions experienced across wind farms and diversity of wind turbine types and capacities. Individual turbines may experience different weather conditions on a given site, and even though the

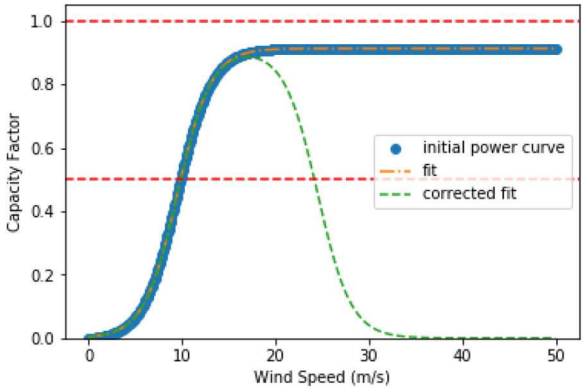

Fig. 3 *Wind farm power curve considering HWSS*

same turbines will have the same, or similar, cut-off and re-connect schemes for extremes of wind, this aggregated impact of across wind farms, never mind on regional, national, or supranational scales, can be challenging to quantify.

5.1 Example methods for determining wind power output

Various different approaches have been tried, but the scarcity of data remains a challenge when it comes to modelling wind farm output in adverse conditions. Examples of work completed in this area can be seen in [11, 30]. In the former, data analysis studied the availability of a wind farm as storm-fronts passed across it to determine the impact of HWSS, whereas in the latter, HWSS was evaluated by generating a power curve from wind speed data compared to aggregated wind power outputs in GB; due to the scarcity of wind speed/output data at high speeds, a Gaussian filter was fitted by inspection to the tail of the data to represent HWSS. This produced a power curve, which was comparable to those described in [31] back in 2009, which discriminated between different types of wind-farm (e.g. onshore, offshore). More ideally representing these phenomena was deemed beyond the scope of this paper. A simple proxy which represents an amalgamation of these and the methods described in [3, 28, 32] is considered.

5.2 Converting wind speed to power output with fitted sigmoidal curve

A curve was fitted to a raw power curve provided by D. Brayshaw from source code referenced in [32] and similar to that deployed in [28], of the following form:

$$y = \frac{a}{1 + \mathrm{e}^{(-f(w)(x - w + \delta))}} \tag{4}$$

a is a normalisation factor set to the value of the maximum of the power curve, and w, $f(w)$ is the power curve represented as an x, y co-ordinate set to which the curve is fitted, with δ shift in the x direction.

Due to the sparsity of data available and the diversity of methods with which to model HWSS, and the nature of the approximations made in similar studies, a proxy was used to represent HWSS based on this curve. A complementary curve was subtracted from the original curve and shifted to change when the curve tends to zero by inspection to match curves produced in similar studies. In effect this assumes the cut-off mechanisms for wind farms that operate in a manner similar to that of the cut-in mechanisms. This produces the curves shown in Fig. 3 with $a = 0.9128$ and $\delta = -15$. Wind power for given wind speeds can then be estimated and visualised in a similar manner to OHL risk. This curve is, by inspection, suitably similar to those used in [30] and in [31] and was deemed appropriate for the applications being used within this work as an indicator of the impact of extreme weather.

6 Case study – GB and SHETL networks

Now that all the data processing methods have been put in place, weather data can be used to visualise risk across the network to help aid planning decisions or resilience studies. This is because the methods shown allow users to target areas of the network either with high probabilities of failure due to extreme wind, or where there would be particularly acute impacts from network outages. A representation of the SHETL region of the GB network was developed using data and input provided by J. Kelly synthesised with network data from the National Grid Electricity Ten Year Statement (ETYS) 2017 [33] and 2018 [34]. The python library *basemap* [35] was used with *matplotlib* [36] and *NetworkX* [37] to visualise the networks and data shown hence. *Pyomo* was also used, but only for data formatting [38].

A severe weather event is chosen – known as 'Cyclone Friedhelm' internationally but known colloquially by a variety of other names within Scotland [39].

First, interpolation was performed on the raw data to improve the granularity of the simulations involved. The data was interpolated linearly to increase the granularity by a factor of 5. The resultant weather grid can be compared with the incident weather in Fig. 4, taken from values in the data set in [24] – the three-level data which allows extrapolation of wind speeds at asset altitudes.

A graphical representation of the developed SHETL network is shown in Fig. 5. It can be observed that much of the network is concentrated in the North and East of Scotland, where much of Scotland's wind production is concentrated. Scotland's wind generation can be seen in Fig. 6, which is generated using data from the Renewables Planning Database (December 2018) [40] with location data converted to latitude–longitude pairs using [41]. Scotland's wind resource can be seen to be distributed, particularly around coastal regions and the borders – much like the transmission network. Using the methods described, the specific weather event can then be investigated.

In order to attain a system-level aggregation of failure probability, a Monte-Carlo simulation is performed using the failure probabilities derived from the weather data, corrected for the altitudes of the assets and the exposure of the line at given points. However, many trials the user desires can be performed depending on the desired balance between computational expense and precision, but 100,000 were chosen for the 132 and 275 kV/400 kV networks. For each trial in the simulation, every section of every line is sampled individually, in turn, assuming an exponential model of failure probability as described in Section 3.2. All lines are assumed in service at the start of each simulation. Theoretically a line could be found to fault in multiple sections simultaneously in each sample hour, or none, hence why it is necessary to sample every section of the line, so these locations are also recorded. The count of total faults recorded in each block across the whole simulation is divided by the sample size to get the probability of a fault happening in each block across the system. This is again an improvement in terms of detail compared to current typical methodologies which, by considering lines as homogenous branches, cannot directly capture this.

A projection of the failure rates corrected for wind speed w.r.t altitude on the 132 and 275 kV/400 kV networks are shown in

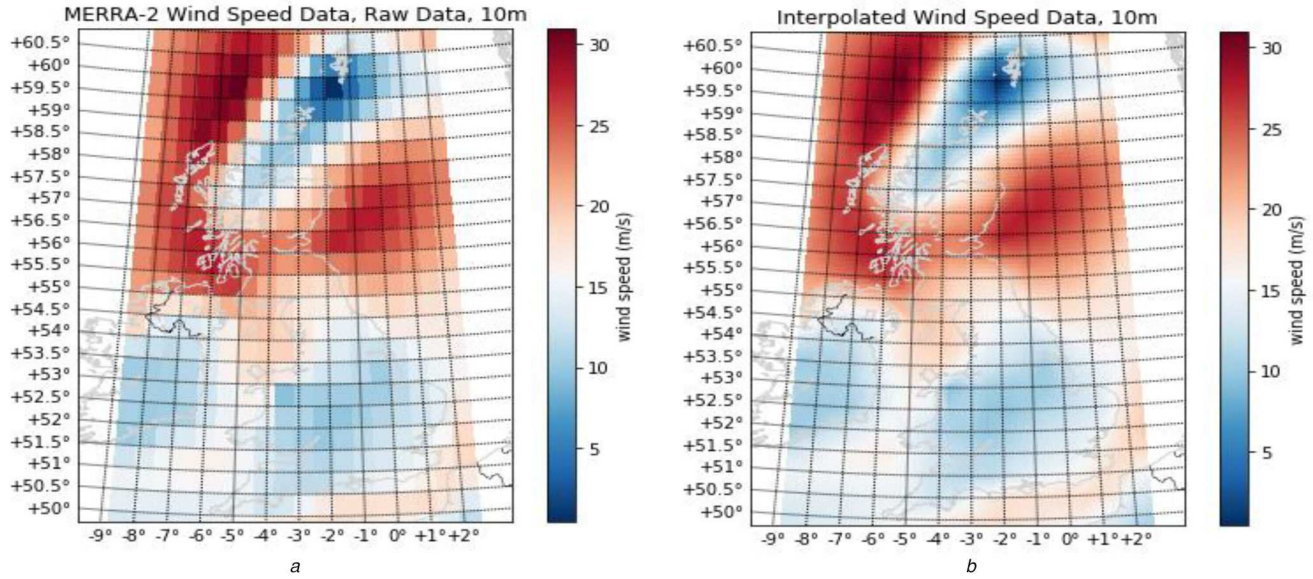

Fig. 4 *Incident weather used in the case study*
(a) Before interpolation, ***(b)*** After interpolation, granularity increased by factor of 5

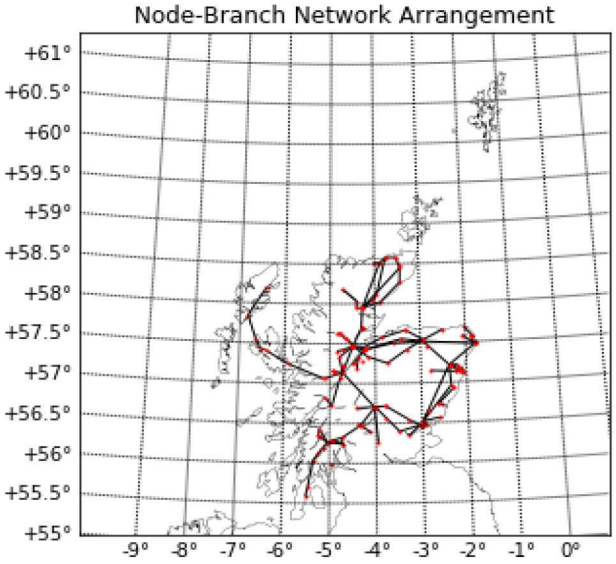

Fig. 5 *Node-branch representation of SHETL network*

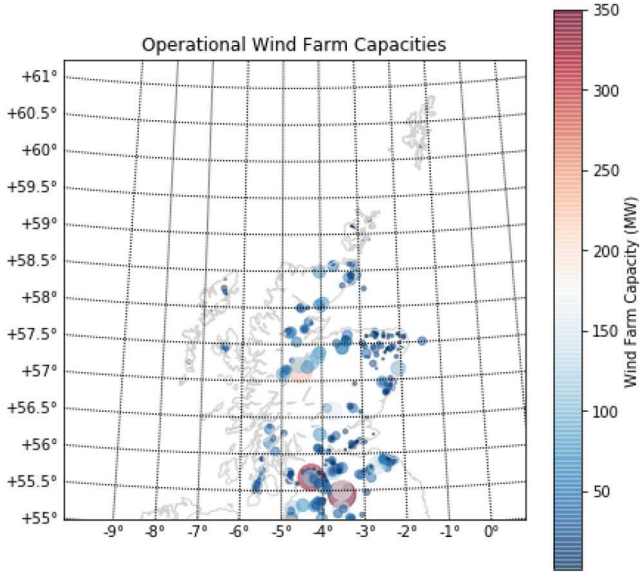

Fig. 6 *Operational wind farm capacities in Scotland, December 2018*

Figs. 7*a* and *b*. Estimated wind production at this time is shown in Fig. 7*d*. Using this data, an estimation of the aggregated line failure probability can be made. This can simply be done by repeating the above process but considering the whole combination of networks, rather than either separately. The mean of the latitude and longitude values at locations at which faults occur are taken to produce a value representative of the expected location of a fault. This is performed using a quicker, 10,000 sample size due to the increasing magnitude of the simulation. This produces the results shown in Fig. 7*c*. The expected fault location (EFL) in this instance is (56.72°, −3.72°). The total estimated wind power output is 2.1 GW in this simulation for the test region.

It can be observed that the 132 kV network, as one would expect, has more extreme values of failure probability than that of the 275/400 kV networks in this case. Further, significant amounts of wind generation, due to HWSS, have zero output, particularly in the South of Scotland, and the highest outputs are barely 50% of the maximum capacities reported in Fig. 6.

The methods described are also applied to a representation of the mainland GB network developed at the University of Strathclyde based on principles described in [42]. A particular feature of this model is that, unlike conventional numerical reductions of larger networks, it attempts to retain details of main transmission routes and of thermal ratings of lines. This was done through keeping lines known by experience to be significant for the operation of the whole system explicitly in the model and collapsing others and the connected generation and demand into equivalents. The results from the SHETL study can then be compared to those for the Reduced GB Network model shown in Fig. 8. A comparison can also be made across the two different data sets – i.e. the three-level set from [25] versus the surface wind speeds uncorrected for altitude taken from the [24] set. Figs. 8*a* and *b* compare the failure probabilities associated with the different data sets. Fig. 8*c* shows the distribution of wind power output across GB for the corrected data. Fig. 8*d* shows the single level incident weather data. The projected wind output map for the single-level data is omitted as it was visually indistinguishable from the corrected wind data map. The EFL for the single level model is (56.00, −3.40)°, and (56.03, −3.26)° for the corrected three-level set. The estimated total wind power is 10.8 GW for the corrected data set, and 11.2 GW for the single level data set. If the raw power curve from Fig. 3 without the correction for HWSS is used, in both cases the estimated wind output across the system is 17.7 GW.

7 Links between elevation, line risk and wind power output

A benefit of disaggregated spatially resolved representations of lines is that more information about local conditions experienced by the system can be ascertained. An example is demonstrated here, pertaining to the estimated local elevation of the grid. Further, as the calculation of 'exposure' thus far has relied on solely 2D point-to-point representation of lines, this has not thus far considered the fact that a line going up and down hills will have more exposure to weather conditions than an equivalent line on a flat surface due to fundamental principles of trigonometry. For example, assuming an ideal, gradual incline from 0 to 1 km elevation on a line going directly East–West in a grid of 5 km × 5 km resolution suggests a 2D representation of that line will underestimate the length of line by ∼2% in that block, assuming the OHL is taut. This was not directly considered in the calculations of line exposure previously.

A plot of the highest sampled elevation in each block is shown in Fig. 9 of the SHETL network model. From this, one can observe that the SHETL network shows significant variation in grid elevation. Presuming the tree-line in the UK is ∼530–600 m, as suggested by [5], significant portions of the network traverse areas both above and below this boundary. Above the tree-line, the lack of trees paired with high wind and heavy rain could contribute to increased risk of landslips. In low-lying areas, substations will be at increased risk of inundation from floodwaters even in urban areas which may have more undergrounding of assets (hence a reduced risk associated with debris or vegetation-related outages on OHL): these may be driven by the same storms. Between the highest elevation of 1099 m and an adjacent block was recorded a difference of 971 m; a 971 m incline over 10 km could mean at least a ∼0.5% difference in estimated exposure between 2D and 3D representation of an OHL on a 10 km × 10 km grid. In situ tracking of this may, therefore, be necessary for future work, particularly for steeper gradients.

Storms associated with the wind not only come with extreme winds but may bring with them heavy rain and flooding conditions. There will, therefore, be risk of flooding in Southerly, low-lying regions with less wind, compounding risk associated with OHL at higher elevations, exacerbated by variability in wind power associated with HWSS.

8 Results and discussion

Considering the elevation and spatial distribution of assets and the altitude of those assets has a minor effect on wind generation output across the network in the given test cases, but has a significant impact on the observed distribution of failure probabilities of OHL on the grid. So too does the depth of model and the network reduction used. Of the 19.5 GW of connected wind in GB, derived from [40], 8.1 GW is connected in Scotland. The estimations of wind power from Scotland in the test case suggest an aggregated output of 2.1 GW (if using the 3-level data) or 2.3 GW of wind infeed on the system (if the simulations represented in Fig. 7 are repeated with the single-level data). Loss

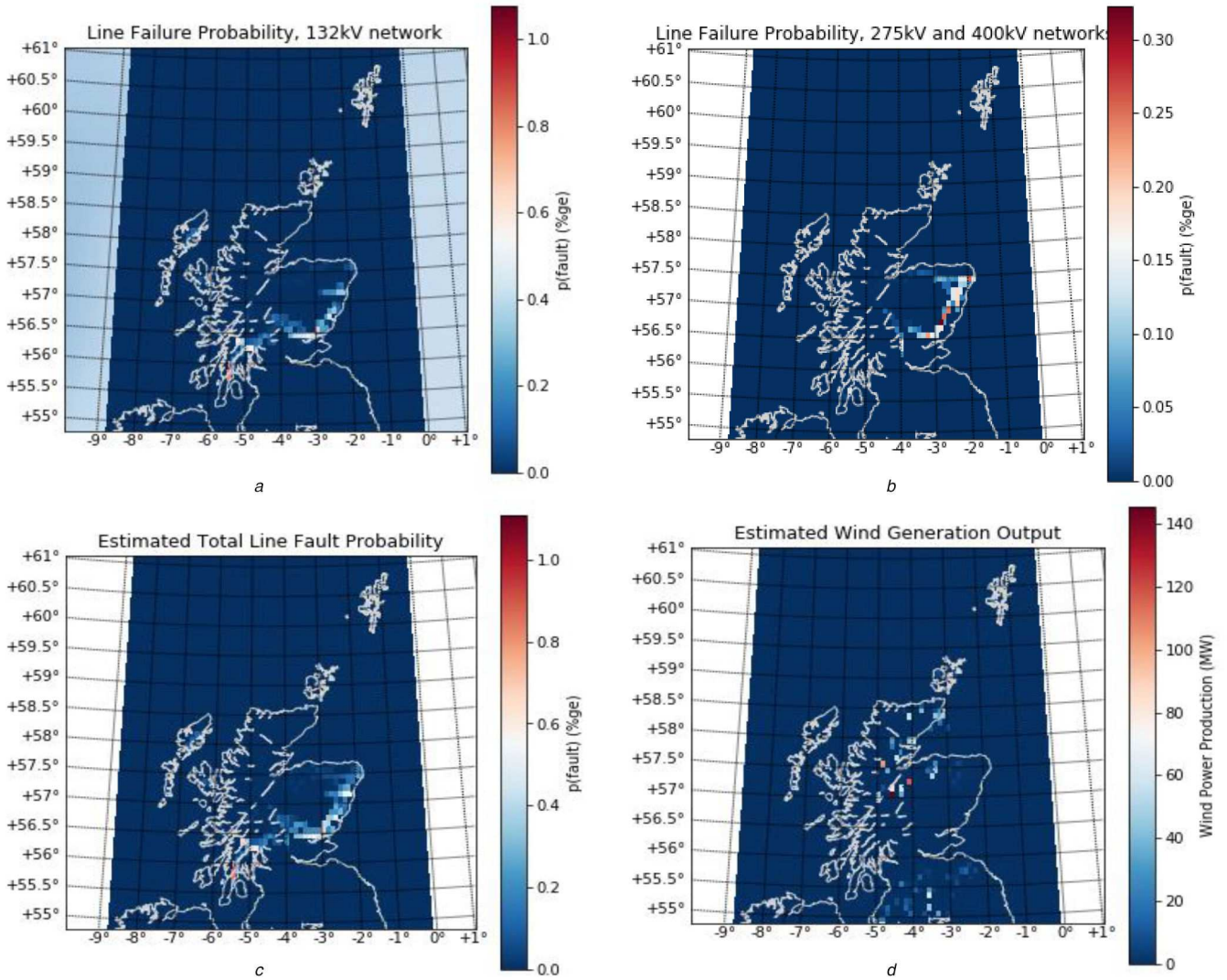

Fig. 7 *Output results for SHETL network*

(a) OHL failure probability on 132 kV network, ***(b)*** OHL failure probability on 275 and 400 kV networks, ***(c)*** Estimated total line failure probability, ***(d)*** Estimated wind production output

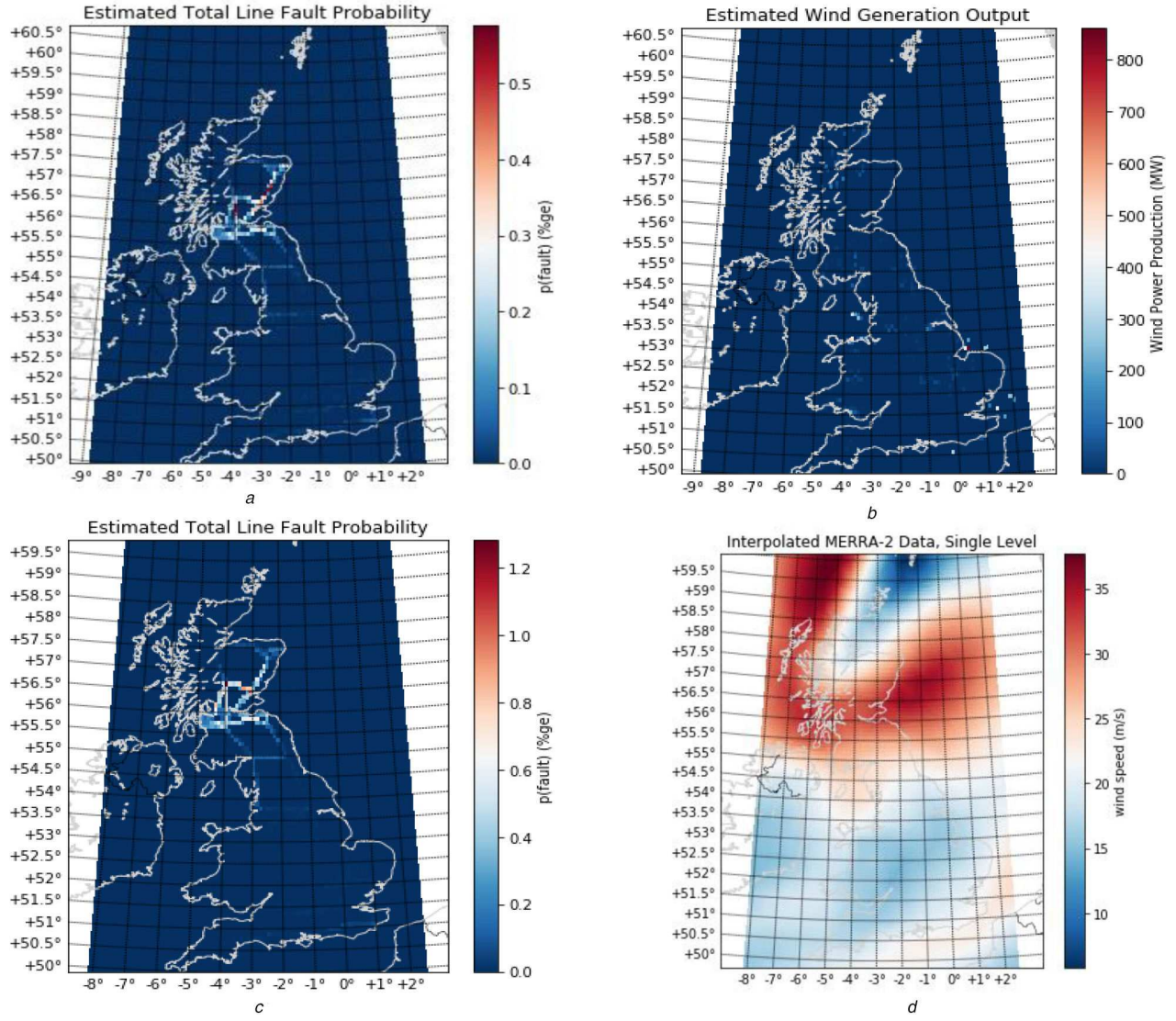

Fig. 8 *Simulation results for the representation of GB network considering different data sets*
(a) Estimated fault probability with weather data corrected for asset altitude, ***(b)*** Estimated wind generation output for weather data corrected for asset altitude, ***(c)*** Estimated line failure probability using single-level, uncorrected data, ***(d)*** Incident single level maximum wind gust speed data

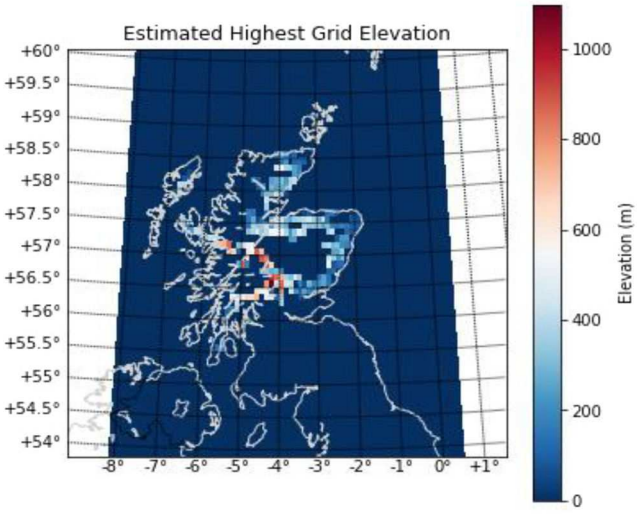

Fig. 9 *The estimated maximum elevation of SHETL network*

of infeed is planned for by system operators, but the risk of HWSS will be compounded by the risk associated with loss of OHL. In Scotland this could affect access to nuclear power from Hunterston and Torness or hydroelectric generation across the Highlands, with significant consequences for wider GB system operability.

'Reduced' network models are common in resilience and reliability studies involving, but not exclusive to, GB, largely due to computational necessity; however, given the complexity of the transmission system and the significantly weaker nature of the 132 kV network compared to the 275 kV/400 kV network, and the

tendency of wind power to be connected to distribution networks, such approximations may be inappropriate for some studies and may significantly overestimate the robustness of such networks. However, such reduction models were not specifically designed for the kind of analyses carried out in this report; rather, the main motivation was to use the network model to explore phenomena and possible innovations to help manage them. The sensitivity of such models to the weather data emphasises the need for spatiotemporally precise data for use in power system simulations, as such data affects both projections about future wind power generation capability and estimations about system resilience.

While storm conditions may cause wind farms in some areas to have high power in-feeds to the grid, as has been demonstrated here, that is very sensitive to the weather conditions and HWSS may cause significant power loss over large geographic areas at times when network capacity is constrained or compromised due to security conditions. Further, since the Scottish network, in particular, may be a net exporter in such conditions, should network degradation reduce export capacity to demand centres in the South, this will have significant impacts well away from the weather system itself. While there may be impacts on Scotland with lost load from weakly-integrated parts of the network, the loss of cross-boundary infeed to the remaining GB network could have major implications. This will be exacerbated given the loss of infeed will simultaneously be at a time of reduced system inertia due to wind power displacing synchronous machines, incurring costs associated either with increased need for frequency reserve or curtailment costs on wind farms. Failure to prepare for such conditions could lead to major outages, cascades, or even widespread blackouts.

The simulations in Fig. 7*c* are repeated with a 10,000 sample size. The wind capacity of farms in Scotland from Fig. 6 are overlain as shown in Fig. 10, with node sizes representing wind farm capacity normalised w.r.t to the largest single wind farm. It can be observed that the greatest line risk overlaps with an important route down which wind power can be transmitted from the North and East of Scotland and in the Southwest. The North–South line in the Centre-West then has increased importance – but it also traverses a significant range of elevations w.r.t Fig. 9, meaning it may be difficult to repair should a fault occur.

It is also worth noting the impact using the single-level data has in comparison to the three-level wind data set. The single-level data has more extreme values throughout the Scottish test area at the 10 m level, but the data is already in the extreme end of wind speed values w.r.t the models being used. That is, around 30 ms^{-1}, the wind power factor is already tailing to zero, concurrently with the failure rate of OHL being severely sensitive to any minor change in wind speed – between 30 and 40 ms^{-1} the failure rate every 100 km/h shifts by approximately an order of magnitude. This is why the two data sets can show significantly different results, even if the general trend remains consistent – that of a high probability of faults in the East Coast and South of Scotland.

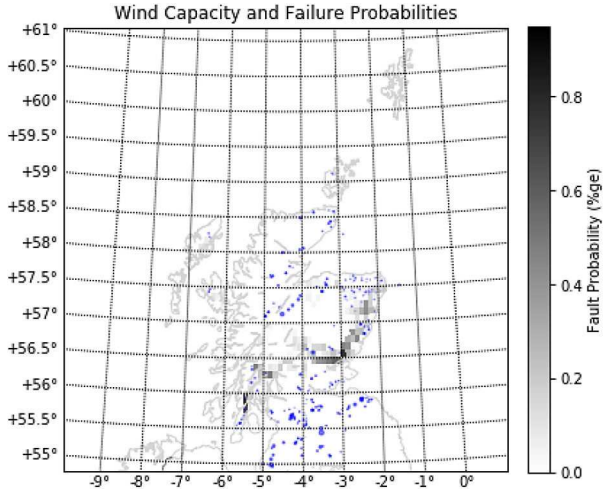

Fig. 10 *Line failure probability and wind farm capacities*

Therefore, in the case study here the failure rate is far more sensitive to changes in the wind speed data – presuming variation is around 25–40 ms^{-1} – as evidenced by the projected wind output changing only by ∼4% between the two data sets for the GB test case compared to the change in failure rate, which almost doubles in regions in the South of Scotland.

Further, it is worth noting that the wind data, while similar, is not a direct comparator with the data on which the fragility curves were formulated. Nevertheless, while being useful for producing a representative indication of risk in this context, the curve as applied here is an imperfect absolute measurement and likely underestimates the true failure risk.

There is only a limited change in the projected wind output because for the most severely affected regions in Scotland wind generation is already a small percentage of its nominal output. This is because of HWSS effects at a time when OHL risk in these areas is concurrently rapidly increasing. Two thresholds then become ostensibly significant in any analysis– circa 20 ms^{-1}, and the tree-line of any region. Beyond 20 ms^{-1} both the models of wind farm output and failure rate on OHLs begin to rapidly change, making them increasingly sensitive to changes in the input data or the corrections made upon it, thus affecting the probability of any outage event and the potential impacts thereof – of course notwithstanding the simplistic representation of HWSS used here. Understanding the elevation of these assets then becomes important because it also shifts the potential mechanics which can cause the failures of assets and the potential error in calculation of OHL exposure to weather.

Simulating the exact same incident event, just using different weather corrections, results in as much as a factor of 2 increase in failure rate on the network and ∼4% change in projected wind output. System risk during extreme wind events, therefore, seems more directly tied to the representation of risk associated with OHL than that linked to HWSS. The two are clearly related, however, though they may manifest differently; HWSS can occur over periods of minutes to hours, whereas network faults can cascade as quickly as protection systems operate. In this case, the storm is relatively localised to Scotland – but wind power across GB is distributed, so though there is significant, localised, risk in Scotland, the projections of wind power in England are not so severely impacted by HWSS or OHL risk.

Resilience analyses have to be extremely careful when examining weather events and using such tools because anything from rounding error to assumptions about asset heights could have profound impacts on the outputs of such models. Similarly, the fragility curves do not account for the potential impact of the direction of the wind on the failure mechanisms on lines. It is reasonable to assume that vegetation related failures could be agnostic of wind direction – a tree falling over on a line or tower could do so from any direction – but it is also reasonable to assume that the failure mechanics associated with a wind direction perpendicular to the bearing of an OHL will differ from that of a gust parallel to it – the fragility curves as implemented cannot yet capture that – and examples were not found in the literature which directly do. It is also likely that, at a distribution level, system assets will be even more vulnerable to high wind speeds than transmission assets – but that remains an area for further study.

Another factor is the granularity and interpolation of the data used. Interpolation of the data can improve the resolution of the maps used to visualise e.g. estimated failure probability, but this still does not account for local topological effects, nor does it account for e.g. coastal effects.

The case study examines 1 test hour based on hourly resolved data, making projections about wind power and failure rates within that hour. For inter-annual or annual simulations, this necessitates a signification increase in computational expense to quantify potential inter-annual variability of failure rates across systems – but these could be particularly targeted, for extreme case studies, at situations where wind speeds approach the values discussed here (particularly beyond 25 ms^{-1}).

Another concern is with the ramping up and down of supply that can occur as storm cycles move across regions, as discussed in detail in [8], which describes potential hourly ramping events of as

much as 15 GW by 2030. This infers significant minute-on-minute variations which are not captured by hourly resolved models such as this but which may need to be captured in resilience studies. The 3-level data used here differs more from the data used in the formulation of the fragility curves relative to the single-level data, and that also has implications for the results. Great care is needed when deciding both the weather data sets used and the fragility curves involved in modelling failure rates. Further, to mitigate the impact of storms such as in the case studies here, future wind generation should be distributed across different regions to prevent HWSS and risk jeopardising wider system security – but should be planned carefully given the relationship between OHL risk and wind power outputs.

9 Conclusion and future work

This paper has proposed methods of presenting OHL risk and the potential effects of HWSS on wind power output and discussed the potential implications of such events using the example of an extreme wind storm from hindcasted data. The method is tractable and could provide operators with a useful tool for resilience planning ahead of similar extreme weather events in the future or be used to hindcast similar events from the past to compare mitigation strategies. It has also been demonstrated how sensitive such models are to the scale of model used and the quality of weather data.

This modelling only considers the risk of the outage on OHLs due to extreme wind, however such fragility curves could also be based on wind and snow events or lightning-related events. The versatility of this approach means those events can also be readily considered and their risks visualised to help planning, particularly pertaining to the location of repair teams and assets. Another potential application of this approach could be to consider the risk associated with line icing or wildfires. Given the links between line loading, line temperature line icing, elevation, and ambient temperature, this approach also offers a foundation on which to investigate such risk in a meaningful way, should the representations used here be linked to load-flow models.

The proposed methods could also be applied to examine impacts of weather conditions on other renewable sources of energy e.g. ambient temperature and solar irradiance on solar generation or precipitation on substation risk and hydroelectric generation; this simply requires changes to the incident weather and relationships with power output, and is another benefit of the proposed approaches.

This work also provides a means to link disparate weather and network analysis tools to analyse weather-related outages and impacts on power systems in a more detailed manner than similar work has provided, and has illustrated the sensitivities involved with using such data.

In geographically diverse regions such as Scotland, taking account of factors such as the wide range of weather conditions which may affect a line of is important given the significant difference in elevations of assets across the grid.

Considering lines in terms of ‘subsections’ with different exposure to weather conditions is a step-change from relying on the homogenous representation of branches. This allows a variety of new and productive results to be ascertained, as shown here with determining the EFL values. The increasing granularity of source data could further improve modelling of line failure risk; interpolation is useful to improve granularity of the simulation but cannot capture many of the features discussed in this report such as coastal effects or effects of changing elevation.

The demonstrated methodology considers variations in line conditions across branches in a robust manner with clear postulated relationships between altitude, exposure, wind speed, and failure rates on lines, and between wind speed and estimated wind power output on farms. The novelty in this work also lies in applying separate fragility curves in the analysis based on voltage level, demonstrating clearly the varied strength of different levels of network and the need to distinguish networks in such a manner. While on a population level a homogenous model for a ‘line’ may well be representative, when performing analysis on a real network the extra granularity used here may be important when simulating events occurring over multiple different voltage levels, particularly as more generation is connected at lower levels.

Applying the method to real networks demonstrates the significance of such relationships in real-world analyses. Further work needs to be done to then weigh the actual impact of these outages on a network to further inform planners, particularly given localised outage events can have distributed effects, by incorporating the modelling with power system simulation models. An immediate example here is that HWSS or network faults in Scotland could lead to cascading outages or major loss of supply to parts of the network far to the South of the areas which are actually impacted by adverse weather conditions. Such work would also need to consider the impacts of e.g. loss of system inertia, network faults, and infeed losses.

An area for improvement could be the granularity of the weather data used to refine the representation of local topological conditions; the tractability of the method means this is straightforward, with the only real limitation being computational expense. The potential benefits of moving from homogenous representations of lines to 2D representations have been shown. A brief investigation into the variation in elevation on the system suggests it is possible – and, on some networks, may be necessary – to move to a 3D representation incorporating elevation. The next step of this work, then, is to link the failure probabilities and power curves utilised here to a simulation model and a representative system model for more comprehensive analysis of risk considerate of both HWSS and risk associated with OHL during storms. It may also be useful to consider 3D representation of OHL using the elevation data acquired. A comparison between the demonstrated approach and conventional, homogenous line representations validated against real data over longer time samples could also be a productive next step for research.

10 Acknowledgments

This work was funded as part of the EPSRC CDT in Future Power Networks and the Smart Grid, based at Imperial College London and the University of Strathclyde. The authors wish to thank Jacob Kelly and Scottish and the Southern Electricity Networks for their contribution to this work, as well as David Brayshaw, Callum MacIver, Rodrigo Moreno and Magnus Davidson for their contributions and support.

11 References

[1] Entriken, R., Lordan, R.: ‘Impacts of extreme events on transmission and distribution systems’. 2012 IEEE Power and Energy Society General Meeting, San Diego, CA, USA, 2012

[2] McColl, L., Palin, E.J., Thornton, H.E., *et al.*: ‘Assessing the potential impact of climate change on the UK's electricity network’, *Clim. Change*, 2012, **115**, (3), pp. 821–835

[3] Brayshaw, D.J., Troccoli, A., Fordham, R., *et al.*: ‘The impact of large scale atmospheric circulation patterns on wind power generation and its potential predictability: a case study over the UK’, *Renew. Energy*, 2011, **36**, (8), pp. 2087–2096

[4] Kuntz, P.A., Christie, R.D., Venkata, S.S.: ‘Optimal vegetation maintenance scheduling of overhead electric power distribution systems’, *IEEE Trans. Power Deliv.*, 2002, **17**, (4), pp. 1164–1169

[5] Backshall, J., Manley, J., Rebane, M.: ‘*The upland management handbook*’ (English Nature Peterborough, UK, 2001)

[6] Napolitano, F., Tossani, F., Borghetti, A., *et al.*: ‘Lightning performance assessment of power distribution lines by means of stratified sampling Monte Carlo method’, *IEEE Trans. Power Deliv.*, 2018, **33**, (5), pp. 2571–2577

[7] ‘Storm Desmond’. Available at https://www.enwl.co.uk/site-search/?q=storm%20desmond#!?page=1, accessed 14 June 2019

[8] Dawkins, L.C.: ‘*Weather and climate related sensitivities and risks in a highly renewable UK energy system: a literature review*’ (The Met Office, UK, 2019)

[9] Energy Research Partnership (ERP). ‘*Future resilience of the UK electricity system*’ (Energy Research Partnership, UK, 2018)

[10] Panteli, M., Mancarella, P.: ‘Modeling and evaluating the resilience of critical electrical power infrastructure to extreme weather events’, *IEEE Syst. J.*, 2015, **PP**, (99), pp. 1–10

[11] Macdonald, H., Hawker, G., Bell, K.: ‘Analysis of wide-area availability of wind generators during storm events’. 2014 Int. Conf. on Probabilistic Methods Applied to Power Systems (PMAPS), Durham, UK, 2014

[12] Billinton, R., Wu, C., Singh, G.: ‘Extreme adverse weather modeling in transmission and distribution system reliability evaluation’. Power Systems Computation Conf. (PSCC), Seville, SPAIN, 2002

[13] Gaver, D.P., Montmeat, F.E., Patton, A.D.: 'Power system reliability I-measures of reliability and methods of calculation', *IEEE Trans. Power Appar. Syst.*, 1964, **83**, (7), pp. 727–737
[14] IEEE Standard 346:1973: 'Terms for reporting and analyzing outages of electrical transmission and distribution facilities and interruptions to customer service', 1973
[15] Clements, D., Mancarella, P.: 'Fragility curve based storm modelling of distribution networks with staff constraints'. IET Int. Conf. on Resilience of Transmission and Distribution Networks (RTDN 2017), Birmingham, UK, 2017
[16] Panteli, M., Mancarella, P., Wilkinson, S., *et al.*: 'Assessment of the resilience of transmission networks to extreme wind events'. 2015 IEEE Eindhoven PowerTech, Eindhoven, Netherlands, 2015
[17] Panteli, M., Mancarella, P.: 'Influence of extreme weather and climate change on the resilience of power systems: impacts and possible mitigation strategies', *Electr. Power Syst. Res.*, 2015, **127**, pp. 259–270
[18] Dunn, S., Wilkinson, S., Alderson, D., *et al.*: 'Fragility curves for assessing the resilience of electricity networks constructed from an extensive fault database', *Nat. Hazards Rev.*, 2017, **19**, (1), p. 04017019
[19] Murray, K., Bell, K.R.W.: 'Wind related faults on the GB transmission network'. 2014 Int. Conf. on Probabilistic Methods Applied to Power Systems (PMAPS), Durham, UK, 2014
[20] Fan, F., Bell, K.R.W.: '*Fragility curves and fault outage prediction for overhead lines*' (University of Strathclyde, UK, 2019)
[21] Jamieson, M., Strbac, G., Tindemans, S., *et al.*: 'A simulation framework to analyse dependent weather-induced faults'. IET Int. Conf. on Resilience of Transmission and Distribution Networks (RTDN 2017), Birmingham, UK, 2017
[22] 'Modern-era retrospective analysis for research and applications, Version 2'. Available at https://gmao.gsfc.nasa.gov/reanalysis/MERRA-2/, accessed 11 April 2019
[23] McKinney, W.: 'Data structures for statistical computing in python'. Proc. of the 9th Python in Science Conf., Austin, TX, 2010
[24] 'MERRA-2 inst1_2d_asm_Nx: 2d, 1-Hourly, Instantaneous, Single-Level, Assimilation, Single-Level Diagnostics V5.12.4'. Available at https://disc.gsfc.nasa.gov/datasets/M2I1NXASM_V5.12.4/summary, accessed 30 March 2019
[25] 'MERRA-2 tavg1_2d_flx_Nx: 2d, 1-Hourly, Time-Averaged, Single-Level, Assimilation, Surface Flux Diagnostics V5.12.4'. Available at https://disc.gsfc.nasa.gov/datasets/M2T1NXFLX_V5.12.4/summary, accessed 17 January 2019
[26] 'SRTM 90 m DEM digital elevation database'. Available at http://srtm.csi.cgiar.org/, accessed 5 April 2019
[27] 'open-elevation'. Available at https://open-elevation.com/, accessed 11 April 2019
[28] Staffell, I., Pfenninger, S.: 'Using bias-corrected reanalysis to simulate current and future wind power output', *Energy*, 2016, **114**, pp. 1224–1239
[29] Jones, E., Oliphant, T., Peterson, P.: 'Scipy: open source scientific tools for python', 2001
[30] Ofgem: 'Electricity capacity assessment report 2013', 2013, pp. 83–84
[31] TradeWind: '*Integrating wind – developing Europe's power market for the large-scale integration of wind power*' (EWEA, Denmark, 2009), pp. 23–25
[32] Cannon, D.J., Brayshaw, D.J., Methven, J., *et al.*: 'Using reanalysis data to quantify extreme wind power generation statistics: a 33 year case study in Great Britain', *Renew. Energy*, 2015, **75**, pp. 767–778
[33] National Grid ESO, 'Electricity ten year statement (ETYS) Appendix A', 2017, pp. 2–8
[34] National Grid ESO, 'Electricity ten year statement (ETYS) Appendix A', 2018, pp. 2–8
[35] 'The Matplotlib Basemap Toolkit User's Guide'. Available at https://matplotlib.org/basemap/users/index.html, accessed 15 April 2019
[36] Hunter, J.D.: 'Matplotlib: a 2D graphics environment', *Comput. Sci. Eng.*, 2007, **9**, (3), p. 90
[37] Hagberg, A., Swart, P., Schult, D.: 'Exploring network structure, dynamics, and function using NetworkX', 2008
[38] Hart, W.E., Laird, C.D., Watson, J.-P., *et al.*: '*Pyomo-optimization modeling in python*' (Springer, Germany, 2012)
[39] 'Scotland hit by 165 mph winds as twitter dubs storm 'Hurricane Bawbag' (Photos) (Video)'. Available at https://www.huffingtonpost.co.uk/2011/12/08/scottish-winds-hurricane-bawbag_n_1136460.html, accessed 15 April 2019
[40] 'Renewable Energy Planning Database quarterly extract'. Available at https://www.gov.uk/government/publications/renewable-energy-planning-database-monthly-extract, accessed 15 April 2019
[41] 'Batch coordinate transformation tool'. Available at https://www.ordnancesurvey.co.uk/gps/transformation/batch#, accessed 3 April 2019
[42] Bell, K.R.W., Tleis, A.N.D.: 'Test system requirements for modelling future power systems'. IEEE PES General Meeting, Minneapolis, MN, USA, 2010